CHAPTER 9

EXCITED-STATE STRUCTURAL DYNAMICS OF NUCLEIC ACIDS AND THEIR COMPONENTS

GLEN R. LOPPNOW*, BRANT E. BILLINGHURST[1],
AND SULAYMAN A. OLADEPO
Department of Chemistry, University of Alberta, Edmonton, AB T6G 2G2 Canada

Abstract: Nucleic acids are the very essence of life, containing the genetic potential of all organisms. However, the sheer size of nucleic acids makes them susceptible to a variety of environmental insults. Of these, ultraviolet-induced damage to nucleic acids has received extensive attention due to its role in disease. The primary step in ultraviolet-induced damage is the absorption of light and the subsequent electronic and structural dynamics on the excited-state potential energy surface. In this chapter, we will review the use of Raman and resonance Raman spectroscopy as a means of obtaining excited-state structural dynamics. Specifically, the application of Raman and resonance Raman spectroscopy to determine the excited-state structural dynamics of nucleic acids and their components will be discussed

Keywords: Excited-State Structural Dynamics, Nucleic Acids, Resonance Raman Spectroscopy, Thymine, Uracil

9.1. INTRODUCTION

9.1.1. Nucleic Acids

Nucleic acids form the essential potential of life. Deoxyribonucleic acid (DNA) carries all of the developmental potential of an organism within its genes. Ribonucleic acid (RNA) has long been thought of simply as an intermediary between DNA and the proteins, which carry out all of the function of the cell. However, recent evidence indicates that RNA may have many other functions, including catalytic and self-catalytic properties [1] and a role in gene expression [2].

* Corresponding author, e-mail: glen.loppnow@ualberta.ca
[1] Current Address: CANMET Energy Technology Centre, 1 Oilpatch Road, Devon, AB T9G 1A8 Canada

M. K. Shukla, J. Leszczynski (eds.), Radiation Induced Molecular Phenomena in Nucleic Acids, 237–263.

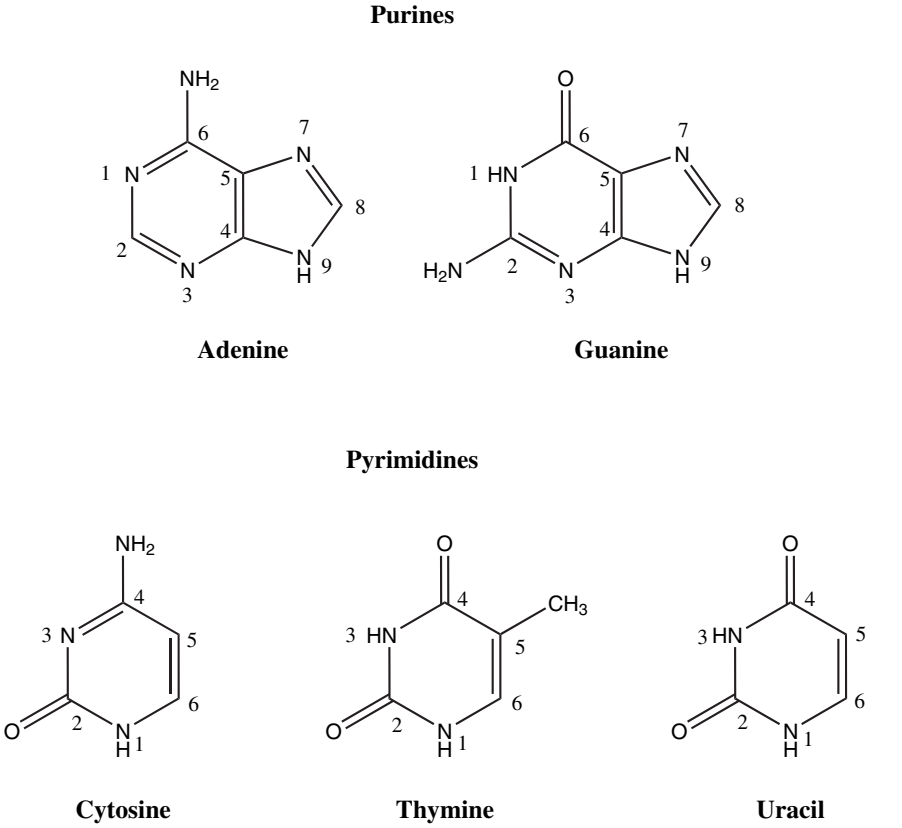

Figure 9-1. Structures and atomic numbering schemes of the five nucleobases. Numbers are given only for the ring atoms

The structures of the nucleobases are shown in Figure 9-1 and the primary structures of DNA and RNA are shown in Figure 9-2. Both nucleic acids are polymers, consisting of an alternating sugar/phosphate backbone and a nucleobase (adenine, cytosine, guanine, thymine and uracil) attached to each sugar. The sugar in RNA is ribose and the sugar in DNA is 2′-deoxyribose. The sugars are connected via phosphate groups bonded to the 3′ carbon of one sugar and the 5′ carbon of an adjacent sugar. Because the phosphate groups have a single negative charge, both DNA and RNA carry a significant negative charge. The nucleobases are usually grouped into the purines (adenine and guanine) and the pyrimidines (cytosine, thymine, and uracil), based on their parent structures. Both RNA and DNA contain the same purines, adenine and guanine. Both RNA and DNA also contain cytosine. However, thymine is used almost exclusively in DNA and uracil is used almost exclusively in RNA.

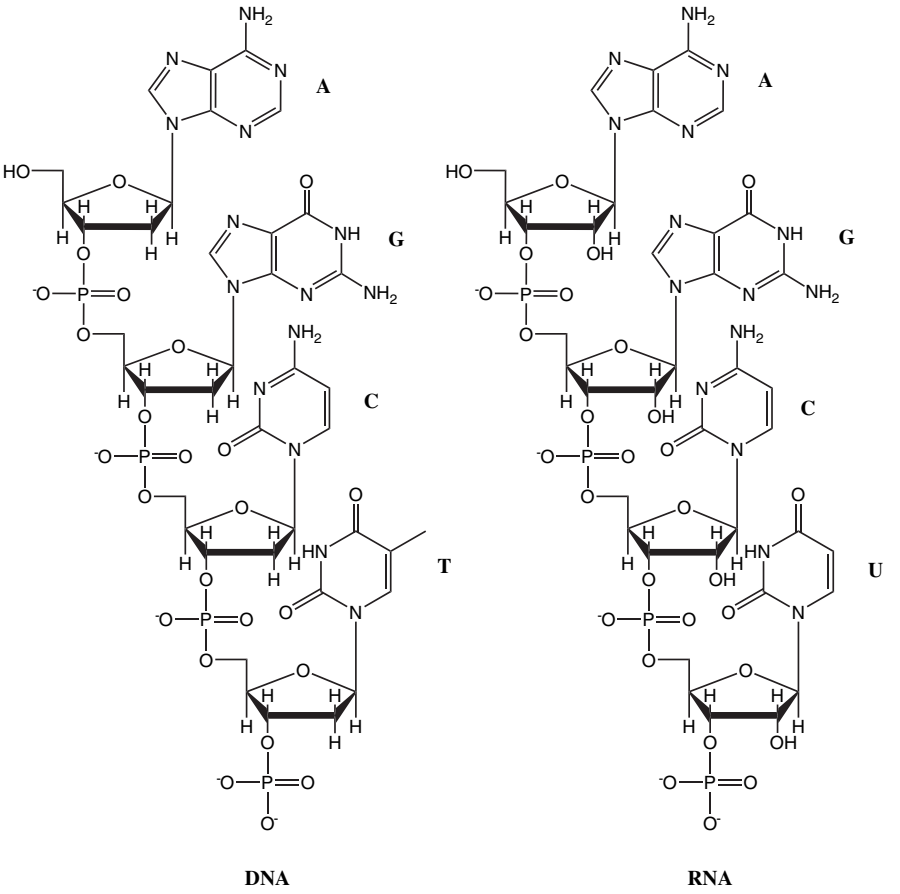

Figure 9-2. Primary structure of DNA and RNA. Letters are the one-letter abbreviation of the nucleobases

Apart from the primary structures of DNA and RNA, they also form distinctive and different secondary structures. DNA is almost always found in the double stranded form, i.e. the nucleobases hydrogen bond to their complementary nucleobases on another strand of DNA. In normal Watson-Crick pairing [3], adenine forms two hydrogen bonds with thymine, and guanine forms three hydrogen bonds with cytosine. This base pairing and the geometry constraints imposed by the glycosidic bond between the sugar and the nucleobase lead to the famous double helix structure of DNA. Surprisingly, this double helix structure is independent of the nucleobase sequence of the DNA. The double helix can take three different forms, A-form DNA, B-form DNA, and Z-form DNA, dependent on the humidity and salt concentration [4]. The most common form at physiological conditions is B-form DNA. A-form and B-form DNA are right-handed helices, while Z-form DNA is

a left-handed helix. An important consequence of the right-handed double helix structure is the resulting stacking of the nucleobases.

In contrast to DNA, RNA is almost always found in the single stranded form. Although, nominally single stranded, different regions of a single RNA strand may base pair, forming such structures as bulges, cloverleaves, hairpin loops and a variety of other structures. Other base-pairing schemes, such as Hoogsteen pairing or guanine tetraplexes, are also possible in DNA and RNA, but will not be discussed further here.

9.1.2. Nucleic Acid Excited-State Electronic Structure

In recent years, the ground-state and excited-state electronic structure of nucleobases and short oligonucleotides has become much clearer. Because other chapters in this book review the experimental, theoretical and computational aspects of nucleobase and oligonucleotide electronic states, only a very brief review will be given here.

A number of researchers, including Kohler [5–13], Gustavsson [14–22], Kong [23, 24], Roos [25–27], Jean [28], Ericksson [29, 30], and others [17, 31–57] have probed the ground and electronic states of nucleobases, nucleosides, nucleotides, and short oligonucleotides with experimental and computational techniques. The consensus is that initial excitation occurs to a state of predominantly ($\pi\pi^*$) character and that the excited states live for a very short time before mostly internal conversion and vibrational relaxation occurs to bring most of the population back to the initial ground state. The most recent measurements cite excited-state relaxation times of τ_1 0.34 ps/ τ_2 0.64 ps for adenine [36], ~100 fs for cytosine [8], 3.2 ps [8] or 0.8 ps [57] or 0.1 ps [8] for guanine, τ_1 0.195 ps/ τ_2 0.633 ps for thymine [8, 14] and 0.096 ps for uracil [8, 14]. Very low (<0.05) quantum yields for triplet formation, photochemistry, and fluorescence are observed in all of the naturally-occurring nucleobases, nucleosides, nucleotides, and larger oligonucleotides. The rapid excited-state relaxation via internal conversion, resulting in the very low quantum yields for other photophysical and photochemical processes, has been cited as one criterion which led to the natural selection of these nucleobases [13, 58]. A number of factors, including base pairing, base stacking, and the presence of other moities on the nucleobase have all been determined to play a role in the excited-state dynamics.

9.1.3. Nucleic Acid Photochemistry

Although the photochemical quantum yields are low, nucleic acids and their components have a rich palette of photochemistry. Different photoproducts are formed dependent on whether the nucleic acid is irradiated with ultraviolet (UV) light or ionizing radiation, and whether the irradition occurs in the presence or absence of oxygen. Since this review is concerned only with UV irradiation, the range of photoproducts is more limited. Figure 9-3 shows most of the primary photoproducts formed in DNA from each of the pyrimidine nucleobases [59]. It should be noted that most of the photochemical mechanisms and quantum yields are dependent on the

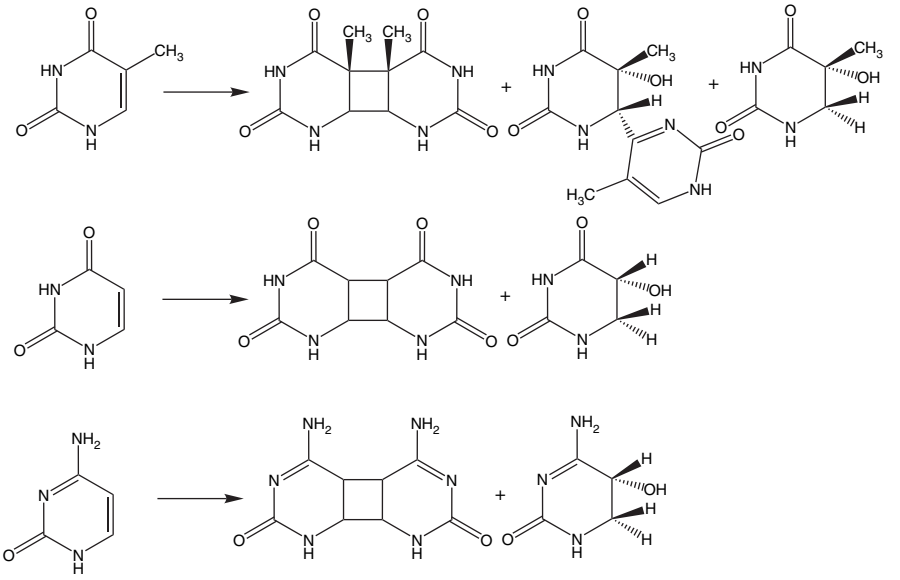

Figure 9-3. Structures of the UV photoproducts of the pyrimidine nucleobases. See text for details

size of oligonucleotide [59]. For example, thymine cyclobutyl photodimer formation proceeds from the monomeric nucleobase with a very low quantum yield via the triplet state in dilute solution, while the quantum yield increases to 0.065 and the mechanism is thought to proceed via the singlet state for 1,3-dimethylthymine in stacked aggregates in more concentrated solutions. Since the photochemistry of DNA has been extensively reviewed [59–64], we will only briefly review the salient points here.

The pyrimidine nucleobases have the highest quantum yields for photoreactivity, with thymine $\sim$ uracil $>$ cytosine. The purine nucleobases have much lower quantum yields for photochemistry, but can be quite reactive in the presence of oxygen. As can be seen from Figure 9-3, thymine forms primarily cyclobutyl photodimers (T<>T) via a $[2\pi + 2\pi]$ cycloaddition, with the *cis-syn* photodimer most prevalent in DNA. This is the lesion which is found most often in DNA and has been directly-linked to the suntan response in humans [65]. A $[2\pi + 2\pi]$ cycloaddition reaction between the double bond in thymine and the carbonyl or the imino of an adjacent pyrimidine nucleobase can eventually yield the pyrimidine pyrimidinone [6–4]-photoproduct via spontaneous rearrangement of the initially formed oxetane or azetidine. This photoproduct has a much lower quantum yield than the photodimer in both dinucleoside monophosphates and in DNA. Finally, thymine can also form the photohydrate via photocatalytic addition of water across the $C_5 = C_6$ bond.

Uracil has a similar photoreactivity to thymine, but in RNA. Although the rate of photoreaction is similar, the photoproduct partitioning is different. While uracil forms the cyclobutyl photodimer and photohydrate, there is no evidence that it forms the pyrimidine-pyrimidinone [6–4] photoproduct. Also, the major photoproduct in

uracil is the photohydrate, not the cyclobutyl dimer as in thymine. The photohydrate has been predicted to form from a zwitterionic excited-state structure [66]. Thus, it is even more surprising that the photohydrate is the major photoproduct in uracil, as the tertiary carbon at C_5 in thymine is expected to stabilize better a carbocation in the zwitterionic excited state. The origin of these differences in photochemistry remains largely unsolved and is one of the motivating factors in the work presented by the authors below.

Finally, cytosine is the least reactive of the pyrimidine nucleobases. It also forms the cyclobutyl photodimer and the pyrimidine-pyrimidinone [6–4]-photoproduct, but no evidence of the photohydrate has been found for cytosine. Cytosine, uracil, and thymine can form heterophotodimers (e.g. T<>C and U<>C) in addition to the homophotodimers. The purines can also participate in photochemical reactions. Some evidence has been found that adenine and thymine can form a heterophotodimer [67]. However, the purines appear to be more susceptible to oxidative damage as a result of their much lower oxidation potentials [68]. Of the purines, guanine is most susceptible and forms primarily 8-oxo-guanine. However, 8-oxo-guanine is somewhat unstable and can rearrange to a number of different products. Because guanine has the lowest oxidation potential of all the nucleobases and acts as an electron sink, it has been implicated as a reactive hotspot in electron transfer models of DNA damage [69, 70].

For all of these types of DNA damage, the initial step in the photochemical reaction is absorption of an ultraviolet photon. The lowest-lying, allowed state is thought to have primarily ($\pi\pi^*$) character for all of the nucleobases [25, 71–76], although there is thought to be one or more ($n\pi^*$) states which are nearly degenerate with the initially excited ($\pi\pi^*$) state. After excitation, an incompletely understood combination of electronic and structural dynamics occurs on the excited state. While significant progress has been made in understanding the electronic dynamics of excited-states, primarily through ultrafast time-resolved absorption and fluorescence spectroscopy (see above), very little is known about the structural dynamics. There are several reasons for this. As mentioned above, the excited state lifetimes of the nucleobases are quite short, typically on the order of a picosecond or less. This short lifetime makes it difficult to resolve the vibrational dynamics before relaxation. The low quantum yields of the photoproducts also make it difficult to distinguish the photochemical reaction dynamics in the excited-state from those that simply lead to relaxation back to the original ground state. Finally, the difficulty of working in the ultraviolet region with ultrafast lasers provides a significant technical challenge in measuring the excited-state structural dynamics. Nevertheless, ultraviolet resonance Raman spectroscopy has provided recent insight into the excited-state structural dynamics and the factors which affect them.

9.1.4. Raman Spectroscopy

Raman spectroscopy is the inelastic scattering of light by the molecular vibrations of the sample (Figure 9-4A). It is similar to infrared (IR) spectroscopy in

that it provides vibrational information, but the Raman light is neither absorbed nor emitted. Indeed, if a transparent sample is illuminated with monochromatic, polarized light, the vast majority of the light is transmitted through the sample and exits unchanged. An additional fraction of the light is scattered, but the wavelength remains unchanged. This light is called Rayleigh scattered light and is the elastic component of the scattered light, i.e. carries no molecular information. The amount of Rayleigh scattered light is dependent on the excitation wavelength and the relative size of the scatterers compared to the wavelength of the excitation light, but does not depend on the molecular vibrations of the sample. Of the light that enters the sample, the tiniest fraction that exits is the inelastically scattered light, i.e. the Raman scattered light. The scattered light can be either higher or lower in energy, depending on whether the molecule is initially vibrationally excited or not. If so, the molecule may give up some energy to the electromagnetic field, resulting in scattered light at higher energy (lower wavelength) than the exciting light. This type of Raman scattering is called anti-Stokes scattering. In anti-Stokes scattering, the Raman intensities depend on the population in the higher-lying vibrational levels, which usually decreases with a Boltzmann dependence for vibrations significantly greater than the approximately 200 cm^{-1} of thermal energy available at room temperature. If the molecular vibrations are all predominantly in their lowest level, the electromagnetic field transfers energy to excite the molecule to a higher-lying vibrational level and the scattered light is at lower energy (higher wavelength) than the exciting light (Figure 9-4A). This latter case is called Stokes scattering and is more typically measured in a Raman spectroscopic experiment.

Classically, Raman spectroscopy arises from an induced dipole in a molecule resulting from the interaction of an electromagnetic field with a vibrating molecule. In electromagnetic theory, an induced dipole is a first-rank tensor formed from the dot product of the molecular polarizability and the oscillating electric field of the photon, $\boldsymbol{\mu} = \boldsymbol{\alpha} \cdot \mathbf{E}$. Assuming a harmonic potential for the molecular vibration, and that the polarizability does not deviate significantly from its equilibrium value (α_0) as a result of the vibration

$$\alpha_k = \alpha_0 + \left(\frac{\partial \alpha}{\partial Q_k} \right)_0 Q_{k0} \cos 2\pi c \tilde{\nu}_k t \tag{9-1}$$

$$E = E_0 \cos 2\pi c \tilde{\nu}_0 t \tag{9-2}$$

where Q_k is the kth normal mode of vibration, Q_{k0} is the normal coordinate amplitude, E_0 is the electric field amplitude of the photon, $\tilde{\nu}_0$ is the incident laser wavenumber, and $\tilde{\nu}_k$ is the vibrational wavenumber. Solving for the induced dipole yields

$$\mu = \alpha_0 E_0 \cos 2\pi c \tilde{\nu}_0 t + \frac{1}{2} \left(\frac{\partial \alpha}{\partial Q_k} \right)_0 Q_{k0} E_0 \left[\cos 2\pi c \left(\tilde{\nu}_0 - \tilde{\nu}_k \right) t + \cos 2\pi c \left(\tilde{\nu}_0 + \tilde{\nu}_k \right) t \right] \tag{9-3}$$

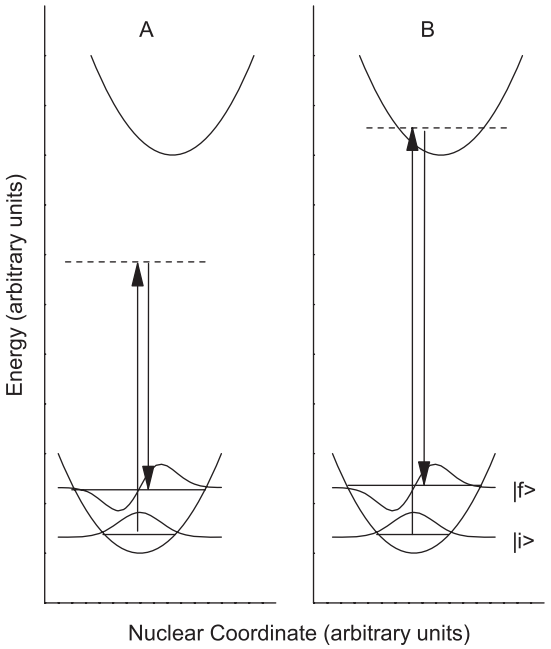

Figure 9-4. The Raman and resonance Raman scattering processes. In this figure, $|i>$ and $|f>$ refer to the initial and final states, respectively, in the Raman or resonance Raman scattering process. (A) In the Raman process, the molecule is initally in its ground vibrational level of the ground electronic state. An excitation photon (*up arrow*) carries the molecule to a virtual level (*dashed line*) from which it immediately scatters inelastically (*down arrow*), leaving the molecule in an excited vibrational level of the ground state. The difference between the excitation and scattered photon is measured. (B) Resonance Raman scattering follows the same process, except that the virtual level (*dashed line*) is coincident with a real excited vibronic level of the molecule. Again, the difference between the excitation and scattered photon is measured

In Eq. (9-3), the first term describes Rayleigh scattering at the incident laser wavenumber, the second term is Stokes Raman scattering at wavenumber $\tilde{\nu}_0 - \tilde{\nu}_k$ and the third term is anti-Stokes Raman scattering at wavenumber $\tilde{\nu}_0 + \tilde{\nu}_k$.

Thus, in the Stokes case, the molecule is initially in its lowest-lying vibrational levels. The incident photon, at an energy much lower than necessary to reach the lowest-lying excited electronic state (i.e. the sample is transparent at this wavelength), excites the molecule to a virtual state (*dashed line* in Figure 9-4A) from which it immediately scatters inelastically. The scattered photon is at lower energy than the exciting photon and the molecule is vibrationally excited in one or more vibrational modes.

Raman vibrational spectroscopy and infrared spectroscopy are usually presented as complementary vibrational techniques because the processes are different, absorption for infrared and scattering for Raman. This difference in process has important consequences that reinforce the idea that infrared and Raman are

complementary spectroscopies. The gross selection rules are different. Infrared intensities are dependent on a change in permanent dipole moment with the vibration, while Raman intensities depend on a change in the polarizability with the vibration. Thus, water is a strong infrared absorber but is a weak Raman scatterer, making Raman spectroscopy much more useful for biological samples. Most functional groups are dipolar, making infrared spectroscopy a very useful technique for the identification of unknown compounds. In fact, this difference yields the mutual exclusivity principle which states that if a molecule contains a center of symmetry, the vibrations that are infrared allowed are Raman forbidden by symmetry and vice versa.

A critical pre-requisite to using Raman and resonance Raman spectroscopy to examine the excited-state structural dynamics of nucleic acids and their components, is the determination of the normal modes of vibration for the molecule of interest. The most definitive method for determining the normal modes is exhaustive isotopic substitution, subsequent measurement of the IR and Raman spectra, and computational analysis with the FG method of Wilson, Decius, and Cross [77]. Such an analysis is rarely performed presently because of the improvements in accuracy of ab initio and semi-empirical calculations. Ab initio computations have been applied to most of the nucleobases, which will be described in more detail below, resulting in relatively consistent descriptions of the normal modes for the nucleobases.

Although both infrared and Raman spectroscopy equipment share the general characteristics of having a light source, wavelength dispersion device and detector, the specific equipment used for infrared and Raman spectroscopy also differs. Infrared spectroscopy is an absorption technique, and therefore requires a light source operating in the infrared region of the spectrum, typically between 15000 and 10 cm^{-1} (667 nm to 1000 μm). Prism and grating monochromators, wavelength dispersion devices for infrared spectroscopy, have been largely supplanted by interferometers and Fourier transform infrared spectroscopy (FT-IR) is commonplace.

Raman vibrational spectroscopy is performed in the visible and near-infrared regions of the spectrum. Since Raman vibrational spectroscopy is a light scattering technique, only the wavelength shift of the scattered light from the excitation wavelength is measured; thus the absolute wavelength of the light is somewhat less important. However, the intensity of scattered light depends on $1/\lambda^4$, so a lower excitation wavelength is useful in most cases. Fluorescence can be a significant interference in Raman spectroscopy, since it occurs in the same spectral region and can be much more intense than the Raman signal. Thus, a judicious choice of excitation wavelength will ensure that the Raman intensities are optimized. Lasers are typically used to provide the excitation in a Raman spectroscopy experiment, as they are highly collimated, monochromatic, polarized sources, ideal for Raman spectroscopy. Grating-based monochromators are used almost exclusively in Raman spectroscopy, usually with one or more filters to remove the higher-intensity Rayleigh scattering. The most popular detectors are charge coupled device (CCD) detectors, but photomultiplier tubes and photodiode arrays are still used.

9.1.5. Resonance Raman Spectroscopy and Excited-State Structural Dynamics

Because of the inherent weakness of Raman scattering, several techniques have been employed to improve the Raman signal. These include coherent Raman scattering, e.g. coherent anti-Stokes Raman scattering (CARS) and coherent Stokes Raman scattering (CSRS), surface-enhanced Raman scattering (SERS), resonance Raman scattering (RRS) and surface-enhanced resonance Raman scattering (SERRS). Of these, only resonance Raman scattering will be discussed, because it yields the excited-state structural dynamics which is the topic of this review.

Resonance Raman vibrational scattering spectroscopy is illustrated in Figure 9-4B. Resonance Raman scattering is essentially the same as Raman scattering, except the energy of the excitation photon is coincident with a vibronic transition in the molecule, i.e. the sample is absorbing at the wavelength of excitation. Although this resonance can lead to a number of undesirable effects, such as increased fluorescence interference, self-absorption of both the excitation and scattered photons, sample heating, and photochemistry, an advantage of the resonance condition is that the Raman signal is significantly enhanced compared to that of unenhanced Raman scattering. It was noticed early on that the relative intensities may also be significantly different in a resonance Raman experiment compared to those obtained off-resonance.

Quantum mechanically, resonance Raman cross-sections can be calculated by the following sum-over-states expression derived from second-order perturbation theory within the adiabatic, Born-Oppenheimer and harmonic approximations

$$\sigma_R = \frac{8\pi e^4 M^4 E_s^3 E_L}{9\hbar^4 c^4} \left| \sum_v \frac{< f|v >< v|i >}{\varepsilon_v - \varepsilon_i + E_0 - E_L - i\Gamma} \right|^2 \tag{9-4}$$

where the resonance Raman cross-section, σ_R, is directly proportional to the absolute measured resonance Raman intensity. In this expression, M is the transition length, E_s and E_L are the scattered and incident photon energies, respectively, $|f>$, $|v>$ and $|i>$ are the final, intermediate, and initial vibrational states, respectively, ε_v and ε_i are the energies of the intermediate and initial vibrational states, E_0 is the zero-zero energy between the lowest vibrational levels of the ground and excited electronic states, and Γ is the homogeneous linewidth [78]. While theoretically elegant, this equation is computationally intensive to evaluate in practice.

Of more utility is the time-dependent analogue of Eq. (9-4), shown in Eq. (9-5) below.

$$\sigma_R = \frac{8\pi E_s^3 E_L e^4 M^4}{9\hbar^6 c^4} \int_0^\infty dE_0 H(E_0) \left| \int_0^\infty < f|i(t) > \right.$$
$$\left. \exp\{i\,(E_L + \varepsilon_i)\,t/\hbar\}\; G(t)\,dt \right|^2 \tag{9-5}$$

In this equation, G(t) is a homogeneous linewidth function, $H(E_0) = (2\pi\Theta)^{-1/2} \exp\{-(< E_0 > -E_0)^2/2\Theta^2\}$ is the inhomogeneous linewidth function

with standard deviation Θ and average energy $<E_0>$, and $|i(t)> = e^{-2\pi\ iHt/h}|i>$ is the initial vibrational wavefunction propagated on the excited-state potential energy surface [78–83]. For molecules interacting with a solvent bath, G(t) represents the dynamics of the chromophore-solvent coupling [84] and takes the form $e^{-g_R(t)-ig_I(t)}$, where $g_R(t) = D^2[e^{-2\pi\Lambda\ t/h} - 1 + 2\pi\Lambda t/h]/\Lambda^2$, D is the coupling strength between the electronic transition and the solvent coordinate, k is the Boltzmann constant, h is Planck's constant, T is the temperature, $h/2\pi\Lambda$ is the characteristic solvent timescale, and $g_I(t) = \pi\ D^2 t/kTh$ in the strongly overdamped, high temperature limit. The inhomogeneous linewidth function is simply a Gaussian distribution of zero-zero energies and assumes the electronic zero-zero energy is more susceptible to solvent interactions.

The absorption cross-section, directly proportional to the molar extinction coefficient ε, is given by

$$\sigma_A = \frac{4\pi E_L e^2 M^2}{6\hbar^2 cn} \int_0^\infty dE_0 H(E_0) \int_{-\infty}^{\infty} dt\ < i|i(t) > \exp\{i\,(E_L + \varepsilon_i)\,t/\hbar\}\,G(t) \tag{9-6}$$

Within the separable harmonic approximation, the $< f|i(t) >$ and $< i|i(t) >$ overlaps are dependent on the semi-classical force the molecule experiences along this vibrational normal mode coordinate in the excited electronic state, i.e. the slope of the excited electronic state potential energy surface along this vibrational normal mode coordinate. Thus, the resonance Raman and absorption cross-sections depend directly on the excited-state structural dynamics, but in different ways mathematically. It is this complementarity that allows us to extract the structural dynamics from a quantitative measure of the absorption spectrum and resonance Raman cross-sections.

The resonance Raman cross-section, σ_R, can be measured experimentally from the resonance Raman intensity by the following equation

$$\sigma_{Nucl} = \sigma_{Std} \frac{I_{Nucl}[Std] E_{Std} L_{Nucl} n_{Nucl} \left(\frac{1+2\rho}{1+\rho}\right)_{Nucl}}{I_{Std}[Nucl] E_{Nucl} L_{Std} n_{Std} \left(\frac{1+2\rho}{1+\rho}\right)_{Std}} 10^{dc(\varepsilon_{Nucl} - \varepsilon_{Std})} \tag{9-7}$$

where σ is the absolute Raman cross-section, I is the resonance Raman intensity, E is the spectrometer efficiency, $L = [(n^2 + 3)/3]^4$ is the internal field correction, n is the refractive index, ρ is the depolarization ratio, d is the Raman sample pathlength, c is the absorbing species concentration, and ε is the molar extinction coefficient. The subscripts Nucl and Std refer to the nucleobase and intensity standard, respectively, present in solution at concentrations [Nucl] and [Std]. If an internal intensity standard is used, $L_{Nucl} = L_{Std}$ and $n_{Nucl} = n_{Std}$. In this method, an internal standard is used whose cross-section has been measured previously. Typical internal standards used are benzene, acetonitrile, cacodylate, sulfate and nitrate.

Besides the sum-over-states and time-dependent models for the resonance Raman cross-section, other models can be used to calculate resonance Raman cross-sections, such as the transform and time correlator models. In the transform model, the resonance Raman cross-sections as a function of excitation energy, the excitation profiles, can be calculated from the absorption spectrum within the separable harmonic oscillator approximation directly by the following relationship [85–87]

$$\sigma_R = \frac{E_L E_s^3 n^2 M^4 \Delta^2}{4\hbar^2 c^2 \pi^3} \left|\Phi(\omega_L) - \Phi(\omega_L - \Omega)\right|^2 \tag{9-8}$$

where Δ is the difference between the ground and excited-state equilibrium geometries for that particular vibrational normal mode, ω_L is the incident laser frequency, Ω is the frequency of the Raman mode of interest,

$$\Phi(\omega_L) = P \int d\omega\, I(\omega)(\omega - \omega_L)^{-1} + i\omega I(\omega_L) \tag{9-9}$$

and

$$I(\omega_L) = \left[\int d\omega/\alpha(\omega')/\omega'\right]^{-1} \alpha(\omega_L)/\omega_L \tag{9-10}$$

where P denotes the principal part of the integral and $I(\omega_L)$ is the normalized absorption spectrum. Thus, the value of Δ for each Raman mode can be obtained directly from the absorption spectrum and the Raman cross-section at a single excitation wavelength. For each vibrational mode, the slope of the excited-state potential energy surface can be easily obtained from Δ within the harmonic oscillator approximation. Note that these expressions do not include inhomogeneous broadening and are strictly correct only for a single molecule. However, deconvolution of the experimental absorption spectrum can be performed prior to the transform to obtain a pseudo-single molecule absorption spectrum. The advantage of the transform method is that the Raman cross-section needs to be obtained at only a single excitation wavelength. Indeed, the Δ for a mode can be obtained from this method simply by measuring the overtone to fundamental ratio in the absence of absolute Raman cross-sections.

The time correlator method [85, 88, 89] has not been used as frequently as the other methods described here, and has not been used for nucleic acids and their components. It will therefore not be discussed further. The experimental methods for determining absolute Raman and resonance Raman cross-sections have been extensively reviewed [90–93]. Similarly, the methods for practical use of the sum-over-states, time-dependent, and transform methods for determining excited-state structural dynamics have been extensively reviewed [78–83].

9.2. NUCLEOBASES

The topic of this review is the excited-state structural dynamics of nucleic acids and their components. As stated above, the excited states of nucleic acid components

are very short-lived, making them difficult to study. Techniques which have been successful at probing the structural dynamics of these short-lived states are UV resonance Raman spectroscopy, computations, and, very recently, time-resolved infrared (IR) spectroscopy. This review will focus mainly on UV resonance Raman determinations of excited-state structural dynamics, but will include discussions of other techniques as appropriate. UV resonance Raman spectra of the nucleobases are shown in Figure 9-5.

Previous reviews of UV resonance Raman spectroscopy applied to nucleic acids and their components were done in 1987 [94] and 2005 [95]. This review will focus exclusively on the application of UV resonance Raman spectroscopy in determining excited-state structure and dynamics of nucleic acids and their components. This review will cover the nucleic acid components first and gradually build up to nucleic acids.

9.2.1. Thymine

One of the most interesting nucleobases in which to study the excited-state structural dynamics is thymine, as thymine photoproducts account for >95% of the lesions found in DNA upon either UVB or UVC irradiation [59]. Excited-state structural

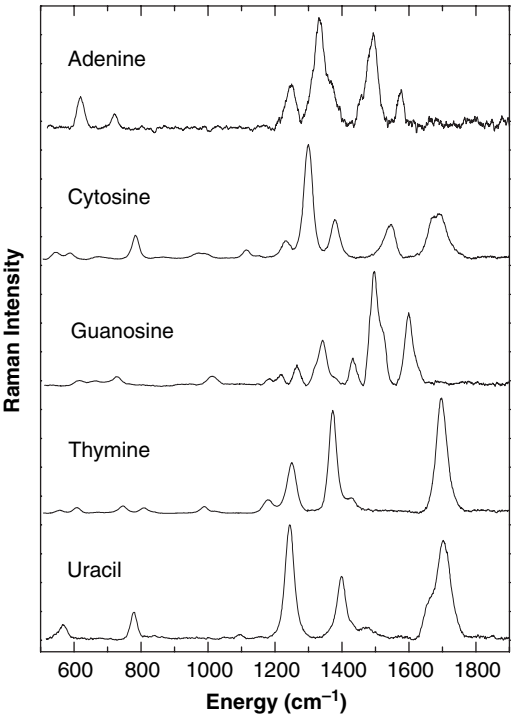

Figure 9-5. UV resonance Raman spectra of the four nucleobases and guanosine excited with 25 mW of 270 nm light. Spectra were obtained as described previously [119], [120], [137], [141], [142]

dynamics occur along the excited-state potential energy surface(s) directly upon absorption of a photon and play a large role in determining the photochemical products and quantum yields.

The ground-state vibrational normal modes of thymine have been extensively studied, both experimentally and computationally. Vibrational spectra of thymine in the polycrystalline state [96–104], in Ar and N_2 matrices [105–109], and in the gas phase [110] have been measured. In the least interactive environments, only the 1-*d*, 3-*d*, and 1,3-d_2 derivatives have been measured, while a number of ^2H and ^{15}N isotopomers in the polycrystalline state have been measured for thymine [104]. Semi-empirical [111, 112] and ab initio [98, 113–115] calculations have been used to assign the vibrational bands for natural abundance thymine. However, the most robust reconciliation of experiment and computation is a recent attempt to computationally reproduce the experimentally observed isotopic shifts in 10 different isotopomers [116] of thymine. The success of that attempt is an indication of the reliability of the resulting force field and normal modes. The resonance Raman vibrations of thymine, and their vibrational assignments, are given in Table 9-1.

With this normal mode description, then, it is instructive to review the resonance Raman intensity-derived excited-state structural dynamics. The first UV resonance Raman study of thymine was not done until 1994 by Lagant, et al. [113], Although Raman and IR spectra of thymine had been recorded much earlier. Most earlier studies of nucleic acid components focussed on the nucleosides and nucleotides. Indeed, much of the earlier research on nucleic acid components was done by the groups of Peticolas and Spiro, working independently. Spiro focussed more on nucleosides and larger nucleic acid structures (see below), while Peticolas examined the nucleobases initially. Peticolas's approach was to combine ab initio computations of the ground-state and excited-state structures and vibrational frequencies, with

Table 9-1. Resonance-enhanced Vibrations of Thymine[a]

Mode (cm^{-1})	Mode Assignment[b]
1662	61 $\nu(C_5C_6) - 13$ be$(C_6H_{12}) - 8\nu(C_6N_1) - 5\nu(C_5C_{11})$
1412	15 $\nu(C_2N_3) - 13\nu(C_4C_5) - 11$ CH_3 umb + 9 be$(N_1H_7) - 8\nu(N_1C_2) + 7$ be$(C_4O_{10}) +$ 7 be$(C_2O_8) - 6$ Ring def 2 − 6 be(N_3H_9)
1359	42 be$(C_6H_{12}) + 12\nu(C_5C_6) + 9\nu(N_1C_2) - 9\nu(C_2N_3)$
1237	29 $\nu(C_5C_{11}) - 21\nu(C_6N_1) - 12$ Ring def 1 + 10 $\nu(N_1C_2) - 10\nu(C_4C_5) - 8\nu(C_2N_3)$
1168	21 $\nu(C_2N_3) + 20$ be$(C_6H_{12}) - 16$ be$(N_1H_7) - 12\nu(N_3C_4) - 11\nu(C_6N_1)$
813	45 Ring def 1 + 20 $\nu(C_5C_{11}) - 11\nu(N_1C_2)$
752	$6\gamma(C_2O_8) - 12$ Ring def 6 + 8 Ring def 4 + 6 $\gamma(C_4O_{10}) - 5\gamma(N_3H_9)$
616	28 be$(C_4O_{10}) - 27$ be$(C_2O_8) + 14$ be$(C_5C_{11}) + 6$ Ring def 2 [6]
563	$9\gamma(N_1H_7) - 6\gamma(N_3H_9)$

[a] Frequencies listed are the experimental frequencies reported here;

[b] Mode assignments from ref. [116]. Abbreviations: ν, stretching; def, deformation; γ, wagging; be, bending; umb, umbrella. Numbers represent the total percentage potential energy distribution (PED) of the listed internal coordinate(s) to the normal mode. Only PEDs greater than 10% have been listed. Positive and negative PEDs represent the phases of the respective internal coordinate contributions.

experimental measurement of the UV absorption spectrum. A transform calculation was performed on the absorption spectrum to yield the UV resonance Raman intensities of the 3N-6 vibrational modes [113, 114, 117, 118]. For thymine, the 6-31G* basis set at the Hartree-Fock level was used for the ground-state and the same basis set was used with the ground-state minimized geometry in a CIS cacluation for the excited-state. The results were encouraging in that the resonance Raman frequencies were accurately calculated. However, the relative resonance Raman intensities did not match well the experimentally-observed resonance Raman intensities [117]. These discrepancies were attributed to a number of possible factors, including calculation inaccuracies and solvent effects, but the lack of absolute cross-section measurements left some ambiguity as to the exact cause.

The UV resonance Raman spectrum of thymine was revisited in 2007, with a slightly different approach, by Yarasi, et al. [119]. Here, the absolute UV resonance Raman cross-sections of thymine were measured and the time-dependent theory was used to experimentally determine the excited-state structural dynamics of thymine. The results indicated that the initial excited-state structural dynamics of thymine occurred along vibrational modes that are coincident with those expected from the observed photochemistry. The similarity in a DFT calculation of the photodimer transition state structure [29] with that predicted from the UV resonance Raman cross-sections demonstrates that combining experimental and computational techniques can be a powerful approach in elucidating the total excited-state dynamics, electronic and vibrational, of complex systems.

Where the results of the experimental and the computational approaches differ for thymine is in the vibrational dynamics near the ground-state equilibrium geometry on the excited-state potential energy surface, the Franck-Condon region. The DFT calculations predict a fairly flat excited-state potential energy surface, while the intense resonance enhancement of the Raman vibrations suggest that a significant slope to the potential energy surface is present along normal modes with large projections on the photochemical reaction coordinate. The latter is more consistent with the rapid excited-state lifetimes of the nucleobases and further suggests that the photochemical and internal conversion reaction coordinates are coincident in thymine. The resonance Raman cross-sections thus support an "early" model of excited-state structural distortions which lead to the photochemical transition state structure. However, greater elucidation of the excited-state potential energy surface will require resonance Raman measurements of at least dinucleotides, to determine whether the presence of the second nucleobase significantly alters the experimental excited-state surface. In this model, then, rapid internal conversion is accomplished by rapid relaxation to lower-lying electronic states which funnel back to the original ground-state equilibrium structure.

9.2.2. Uracil

Uracil replaces thymine as the fourth nucleobase in RNA and is a common damage product in DNA and RNA from the deamination of cytosine. The physiological

consequences of uracil photochemistry have not been studied as extensively as those of thymine, as RNA is more difficult to work with, given its inherent chemical lability. Nevertheless, uracil provides a fascinating case study for understanding the determinants of excited-state structural dynamics and the resultant photochemistry, given its structural analogy to thymine and, yet, its inexplicably strict separation from thymine in biology to RNA.

The ground-state vibrational normal modes of uracil have also been extensively studied, both experimentally and computationally. The IR and Raman spectra in Ar matrix have been measured for the 5-*d*, 6-*d*, 5,6-d_2, 1,3-d_2, 1,3,5-d_3, 1,3,6-d_3, and d_4 isotopomers [120–122]. Vibrational spectra in the crystalline phase have been reported for the 5,6-d_2, 1,3-d_2, and d_4 isotopomers of uracil [123] and of the 2-^{18}O, 4-^{18}O, 3-*d*, 5-*d*, 6-*d*, 5,6-d_2 and 1-methyl-d_3 isotopomers of 1-methyluracil [124]. UV Resonance Raman spectra have been reported for natural abundance, 2-^{18}O, 4-^{18}O, and 2,4-$^{18}O_2$ uracil in neutral aqueous solution [125]. These data have been modeled successfully by both ab initio [94, 117, 126–132] and semi-empirical [133, 134] calculations. However, most of these caculations ignore electron correlation effects on the vibrational properties of uracil, particularly the Raman and resonance Raman spectra. However, the most robust reconciliation of experiment and computation is a recent attempt to computationally reproduce the experimentally observed isotopic shifts in 4 different uracil isotopomers [116]. The success of that attempt is an indication of the reliability of the resulting force field and normal modes for uracil. The resonance Raman vibrations of uracil, and their vibrational assignments, are given in Table 9-2.

Much of the early UV resonance Raman spectroscopy and determination of the excited-state structure of uracil was also performed by Peticolas [96, 113, 114, 117, 118], using a similar approach to that described above for thymine. In addition to uracil, the calculated and experimental UV resonance Raman spectra of 1-methyluracil and

Table 9-2. Resonance-enhanced Vibrations of Uracil[a]

Mode (cm^{-1})	Mode Assignment[b]
1664	71 $\nu(C_4O_{10})$ − 8 $\nu(C_4C_5)$ + 5 ring def 2
1623	61 $\nu(C_5C_6)$ − 14 be(C_6H_{12}) − 8 $\nu(C_6N_1)$
1388	18 $\nu(C_2N_3)$ + 17 be(N_3H_9) − 15 $\nu(N_1C_2)$ + 13 be(C_5H_{11}) − 12 be(C_6H_{12}) − 8 $\nu(C_5C_6)$ + 5 be(C_4O_{10})
1235	33 be(C_5H_{11}) + 18 be(C_6H_{12}) − 15 $\nu(C_6N_1)$ + 10 be(N_1H_7) + 7 $\nu(N_3C_4)$ + 5 $\nu(N_1C_2)$
1093	33 $\nu(C_6N_1)$ + 23 be(C_5H_{11}) + 9 $\nu(C_5C_6)$ − 9 $\nu(N_3C_4)$ − 6 $\nu(N_1C_2)$
789	45 $\gamma(C_2O_8)$ + 29 Ring def 4 − 12 $\gamma(N_3H_9)$
579	84 $\gamma(N_1H_7)$ − 6 $\gamma(C_5H_{11})$ − 5 $\gamma(C_4O_{10})$

[a] Frequencies listed are the experimental frequencies reported here;

[b] Mode assignments from ref. [116]. Abbreviations: ν, stretching; def, deformation; γ, wagging; be, bending. Numbers represent the total percentage potential energy distribution (PED) of the listed internal coordinate(s) to the normal mode. Only PEDs greater than 10% have been listed. Positive and negative PEDs represent the phases of the respective internal coordinate contributions.

the 1,3-dideuterio isotopomers of each were also compared. The results show that the ab initio + transform strategy for finding the UV resonance Raman spectra-and, in the process, confirming the excited-state structural dynamics predicted from the ab initio computations-works well for the deuterated species, but does not predict well the UV resonance Raman spectra of the parent species. This discrepancy was attributed to vibrational resonances involving the N_3-H bending motion [114].

The UV resonance Raman cross-sections and experimentally derived excited-state structural dynamics of uracil were measured independently in 2007 by Yarasi, et al. [119]. The results indicate that the initial excited-state structural dynamics of uracil are significantly different than those in thymine and occur along vibrational modes that are delocalized over the entire molecule, rather than localized at the photochemically active $C_5 = C_6$. This rather surprising result, given the structural similarities between uracil and thymine, was attributed to the effect of a large mass at C_5 which localized the vibrations [119] more in thymine than in uracil. This model has been confirmed in a number of analogues of uracil with various heavy substituents at C_5, yet all show similar UV resonance Raman spectra (see below). The similarity in ab initio multireference configuration interaction calculations of the excited-state potential energy surface of uracil [135, 136] with that predicted from the UV resonance Raman cross-sections demonstrates that combining experimental and computational techniques can be a powerful approach in elucidating the total excited-state dynamics, electronic and vibrational, of complex systems. In particular, the theoretical prediction and experimental verification of non-zero slopes along various vibrational modes in the excited-state potential energy surface is consistent also with the rapid excited-state lifetime of uracil.

The difference in excited-state structural dynamics between uracil and thymine leads to a different model for the photochemistry in these two nucleobases. In thymine, the initial excited-state structural dynamics, derived from the resonance Raman intensities, have a large projection along the photochemical reaction coordinate. In this "early" model of the photochemistry, the photochemical yields would be quite high, except for the rapid deactivation of this excited electronic state back to the original ground state via facile internal conversion processes. A different picture emerges for the photochemistry of uracil. In uracil, the initial excited-state structural dynamics do not have a large projection along the photochemical reaction coordinate. In fact, the majority of the excited-state structure distortion appears along delocalized modes, as if the energy is being dissipated. Thus, the excited-state structural dynamics which yield the photohydrate major product and photodimer minor product must occur "late" on the excited-state potential energy surface. Further experimental probing of the excited-state structural dynamics is necessary to further elucidate the mechanism of photohydrate formation.

9.2.3. Cytosine

Much less UV resonance Raman work has been done on cytosine than the other pyrimidine nucleobases. Only Billinghurst and Loppnow [137] have determined the

excited-state structural dynamics for cytosine bases from the UV resonance Raman intensities. They found that the structural dynamics for cytosine were intermediate between those of thymine and uracil, perhaps accounting for the intermediate nature of the photochemistry; cytosine forms the photodimer as the major product, but the photohydrate is the minor photoproduct.

9.2.4. Pyrimidine Derivatives

Peticolas [113, 114, 117, 118, 138], Spiro [139] and Harada [140] have all looked at the UV resonance Raman spectra of pyrimidine derivatives. Spiro and Harada focused mainly on ground state properties, identification and solvent affects on frequencies, respectively. Peticolas's focus was primarily on developing a robust force field for the pyrimidine nucleobases, by using the UV resonance Raman intensities as a check on the validity of the force field. As described above, this effort resulted in good simulations of the UV resonance Raman spectra of the deuterated pyrimidine nucleobases, but relatively poorer simulations of the naturally-occurring nucleobase spectra. A more recent calculation of the vibrational assignments using DFT methods at the B3LYP level with the 6-31G(d,p) basis set shows that the natural abundance and isotopomer vibrational frequency shifts for both uracil and thymine can be accurately calculated [116]. This recent calculation shows a difference in vibrational assignment from the earlier calculations in the fingerprint (500–1400 cm^{-1}) region of the Raman spectrum, which may explain why some of the UV resonance Raman intensities in the earlier calculation were inaccurately simulated. Very recently, Fraga, et al. [141] have used UV resonance Raman spectroscopy to determine the excited-state structural dynamics of 1-methylthymine. The results indicate a substantial change in the vibrational assignments compared to thymine, and some delocalization of the dynamics over the entire molecule. Thus, the excited-state structural dynamics are more similar to those found in uracil, than those found in thymine. This was attributed to the lower frequencies of the N-methyl group vibrations, compared to the normal proton vibrations at N1, facilitating greater coupling of the N-methyl group with the ring vibrations. Thus far, no determination of the excited-state structural dynamics of isotopically-substituted pyrimidine nucleobases has been performed.

UV resonance Raman spectra of chemical analogues of the pyrimidine nucleobases have been recently reported. Billinghurst et al. [142] have recently reported the UV resonance Raman intensity-derived excited-state structural dynamics of 5-fluorouracil, and have shown them to be essentially identical to those of thymine. In that paper, they also report the UV resonance Raman spectra of 5-chlorouracil, 5-bromouracil, and 5-iodouracil, and show that the spectra all are similar. By extension, they argue that the excited-state structural dynamics of the 5-halouracils are all similar to each other and to those of thymine, supporting their model that the excited-state structural dynamics of uracil and thymine nucleobases are dictated by the mass of the substituent at the 5 position.

9.2.5. Purines

Very few reports of the excited-state structural dynamics of the purine nucleobases have appeared in the literature. This lack of research effort is probably due to a number of factors. The primary factor is the lack of photochemistry seen in the purines. Although adenine can form photoadducts with thymine, and this accounts for ~0.2% of the photolesions found upon UVC irradiation of DNA [67], the purines appear to be relatively robust to UV irradiation. This lack of photoreactivity is probably due to the aromatic nature of the purine nucleobases. A practical issue with the purine nucleobases is their insolubility in water. While adenine enjoys reasonable solubility, it is almost an order of magnitude lower than that of thymine and uracil, the two most soluble nucleobases [143]. Guanine is almost completely insoluble in water at room temperature [143].

Nevertheless, a few reports of UV resonance Raman spectra of the purine nucleobases and their derivatives have appeared. Peticolas's group has reported the identification of resonance Raman marker bands of guanine, 9-methylguanine and 9-ethylguanine for DNA conformation [118, 144]. In the process of doing that work, very rudimentary excitation profiles were measured, which yielded preliminary structures for two of the ultraviolet excited electronic states. Tsuboi has also performed UV resonance Raman on purine nucleobases in an effort to determine the resonance enhanced vibrational structure [94]. Thus far, no excited-state structural dynamics for any of the purine nucleobases have been determined.

9.3. NUCLEOSIDES AND NUCLEOTIDES

In contrast to the isolated nucleobases, a significant amount of work has been done on the excited-state structural dynamics and UV resonance Raman spectroscopy of the nucleotides. The excited-state structural dynamics of nucleosides have not been determined to date, although some UV resonance Raman spectra of the nucleosides have been measured [139, 145, 146]. This work on the nucleosides has been primarily for the application of UV resonance Raman spectroscopy in the determination of ground-state structure, rather than excited-state structural dynamics. This emphasis on the nucleotides is no doubt driven by their greater solubility, as well as their immediate relevance to the nucleic acids. In addition, it was believed that the vast majority of the intensity observed in the UV Raman spectra arose through resonance enhancement of the nucleobase chromophore. Much of the early work on the UV resonance Raman spectra of nucleotides and nucleosides was completed by the groups of Tsuboi, Spiro and Peticolas.

The vibrational structure of the nucleosides and nucleotides has been a subject of great research effort. The early work on the vibrational structure of nucleosides performed up to 1987 has been extensively reviewed [94]. The net conclusion was that the vibrational modes of the nucleosides are essentially unchanged from those of the nucleobase chromophore, i.e. the sugar contributes very little to the resonance enhanced vibrations of the nucleobase chromophore. More recent work [144, 145]

has shown that, in fact, the sugar vibrations of thymidine are coupled to those of the thymine nucleobase, even in resonance with the 260 nm absorption band. Nevertheless, the most intense resonance Raman vibrations appear to derive all of their intensity from the nucleobase chromophore alone [141].

Peticolas was the first to measure the UV resonance Raman spectrum and excitation profile (resonance Raman intensity as a function of excitation wavelength) of adenine monophosphate (AMP) [147, 148]. The goal of this work, besides demonstrating the utility of UV resonance Raman spectroscopy, was to elucidate the excited electronic states responsible for enhancement of the various Raman vibrations. In this way, a preliminary determination of the excited-state structures and nature of each excited electronic state can be obtained. Although the excited-state structural dynamics could have been determined from this data, that analysis was not performed directly.

This initial report was followed closely by the UV resonance Raman spectra of uridine (UMP), cytidine (CMP) and guanidine (GMP) monophosphates by Nishimura, et al. [149] and the application of UV resonance Raman spectroscopy to nucleic acids and their components started in earnest. In the years that followed, Peticolas and Spiro provided much of the research effort in this area. For nucleosides and nucleotides, Peticolas studied guanosine [150], UMP [151–154], GMP [152, 155], AMP [144, 152, 156] and CMP [153]. Spiro was the only one to measure the UV resonance Raman spectra of TMP, in addition to those of all the other naturally occurring nucleotides [157, 158]. For all of these nucleotides, UV resonance Raman excitation profiles have been determined.

What is remarkable is that all of these early measurements of the UV resonance Raman spectra of nucleic acid components involved computational and theoretical support to their experimental findings. For example, Spiro used CINDO calculations to determine the nature of the excited electronic states of the nucleotides [157]. In the early and mid 1970's, many researchers were also attempting to understand resonance Raman spectroscopy, the types of information it could provide, and a unifying theoretical framework to the intensities [147, 159–172]. UV resonance Raman spectra provided some of the first experimental evidence to test the various theoretical models. Peticolas attempted to fit the observed experimental excitation profiles of AMP [156], UMP [151, 154] and CMP [152, 153] to the sum-over-states model for the resonance Raman cross-sections. From these simulations, they were able to obtain preliminary excited-state structural dynamics of the nucleobase chromophores of the nucleotides for UMP [151, 153, 158] and CMP [153]. For AMP, the experimental excitation profiles were simulated with an A-term expression, but the excited-state structural changes were not obtained. Rather, the goal of that work was to identify the electronic transitions within the lowest-energy absorption band of adenine [156].

The major excited-state structural dynamics observed in UMP [173] were ascribed to modes at 1231, 783, 1680, 1396, and 1630 cm^{-1}, in that order, while the major excited-state structural dynamics in the isolated chromophore occur along the 1231, 1680, 1396, and 1630 cm^{-1} modes in that order, with very minor contributions

from modes below 1000 cm^{-1}. Thus, the only difference is the contribution of the 783 cm^{-1} mode, which may carry a significant vibrational contribution from the sugar in the nucleotide [94]. Therefore, the excited-state structural dynamics of UMP appears to be dominated by the excited-state structural dynamics of the uracil nucleobase chromophore.

In CMP, the excited-state structural dynamics were ascribed to modes at 784, 1243, 1294 and 1529 cm^{-1} [153], in that order, while the major excited-state structural dynamics in the isolated nucleobase chromophore occur along the 1283, 1364, 1651, 1523, 1224, and 1630 cm^{-1} modes [137], in that order; again, very minor contributions to the excited-state structural dynamics are observed from the modes below 1000 cm^{-1}. Here, the excited-state structural dynamics of the nucleotide appear to be very different from those of the cytosine nucleobase. A resolution to those discrepancy between the excited-state structural dynamics of the nucleobase and nucleotide awaits definitive vibrational assignments of these modes in cytosine.

Although the excitation profiles of TMP [157] are known, no attempt has been made to extract the excited-state structural dynamics of these nucleotides until recently [141]. This paucity of data is somewhat surprising, given the importance of thymine photochemistry in DNA damage mechanisms. For TMP, the significant excited-state structural dynamics occur along the 1663, 1376, and 1243 cm^{-1} modes, with minor contributions from the other modes. These modes are tentatively assigned as arising from vibrations solely of the thymine chromophore [141], although it is somewhat unclear yet what the contributions to the resonance-enhanced Raman vibrations are from the sugar and/or phosphate group of the nucleotide.

The excitation profile of GMP is also known [157], but no reports of excited-state structural dynamics for GMP have appeared in the literature. GMP can also play a role in DNA damage, particularly in the presence of oxygen, where it forms 8-oxo-deoxyguanosine [174]. For GMP in the ca. 260 nm absorption band, the most intense resonance Raman bands are observed at 1489, 1578 cm^{-1}, with more minor bands at 1326, 1603 and 1364 cm^{-1}, suggesting that these are the modes along which the major excited-state structural dynamics occur. The most intense modes have been assigned to out-of-phase combinations of a C_8H deformation + N_9C_8 stretch and a C_4N_3 stretch + C_5C_4 stretch, respectively, of the guanine nucleobase chromophore. The excited-state structural dynamics at C_8 may explain the formation of the 8-oxo-deoxyguanosine photoproduct. Again, a precise description of the normal modes of vibration of GMP is required to definitively describe the excited-state structural dynamics.

9.4. OLIGONUCLEOTIDES

Much Raman and UV resonance Raman work has been done on polynucleotides and oligonucleotides. Raman spectroscopy of polynucleotides has been used to examine the conformation [95, 175] and melting of oligodeoxyribonucleotides [176].

A number of marker bands have been identified to correlate with conformation, base stacking and base pairing, and this topic has been reviewed recently [95]. UV resonance Raman spectroscopy has also been used to examine the conformation [177, 178], base stacking [177, 179], melting [180] and base pairing [146, 177, 181] of natural and artificial oligodeoxyribonucleotides [95]. Much less work has been done on the oligoribonucleotides, probably because of their chemical lability and slightly more difficult synthesis. Most authors comment on the hypochromism present in the UV resonance Raman spectrum. Because the resonance Raman intensities are approximately proportional to ε^2, the square of the molar extinction coefficient, hypochromic effects will decrease the resonance Raman intensities proportionately more than the decrease in absorbance.

A few of these UV resonance Raman studies have reported excitation profiles of oligonucleotides [158, 177]. These studies show that the hypochromism in the resonance Raman intensities can be as large as 65% for bands enhanced by the ca. 260 nm absorption band for poly(dG-dC) and that the hypochromism can vary substantially between vibrational modes [177]. In the duplex oligonucleotide poly(rA)-poly(rU) [158], similar hypochromism is seen. Although the UV resonance Raman excitation profiles of oligonucleotides have been measured, no excited-state structural dynamics have been extracted from them.

Thus far, the only excited-state structural dynamics of oligonucleotides have come from time-resolved spectroscopy. Very recently, Schreier, et al. [182] have used ultrafast time-resolved infrared (IR) spectroscopy to directly measure the formation of the cyclobutyl photodimer in a $(dT)_{18}$ oligonucleotide. They found that the formation of the photodimer occurs in $\sim$1 picosecond after ultraviolet excitation, consistent with the excited-state structural dynamics derived from the resonance Raman intensities. They conclude that the excited-state reaction is essentially barrierless, but only for those bases with the correct conformational alignment to form the photoproducts. They also conclude that the low quantum yields observed for the photodimer are simply the result of a ground-state population which consists of very few oligonucleotides in the correct alignment to form the photoproducts.

9.5. DNA AND RNA

Thus far, only one report of the UV resonance Raman excitation profiles of nucleic acids has appeared in the literature. The excitation profiles of calf thymus DNA [177] shows the same hypochromism as that observed in both single-stranded and duplex oligonucleotides. Also as expected, the excitation profiles are quite complex. Although an excitation profile is obtained for every vibrational mode, numerous bases are contributing to the Raman intensity observed in every vibration, each in its own microenvironment. Thus, the resonance Raman intensities currently are not useful for elucidating the excited-state structural dynamics of nucleic acids.

9.6. CONCLUSIONS

The determination of excited-state structural dynamics in nucleic acids and their components is still in its infancy. Although progress has been made in understanding the excited-state structural dynamics of the nucleobases, primarily with UV resonance Raman spectroscopy, much work still remains to be done at that level to be able to extract the structural determinants of the excited-state structural dynamics and resulting photochemistry. Much less is known about the excited-state structural dynamics of nucleotides, oligonucleotides, and nucleic acids, but the static and time-resolved spectroscopic tools exist to be able to measure them.

REFERENCES

1. Zaug AJ, Been MD, Cech TR (1986) Nature 324: 429.
2. Chakraborty C. (2007) Curr. Drug Targets 8: 469.
3. Watson JD, Crick FHC (1953) Nature 171: 737.
4. Saenger W (1984) Principles of nucleic acid structure, Springer-Verlag, New York, p 556.
5. Blancafort L, Cohen B, Hare PM, Kohler B, Robb MA (2005) J Phys Chem A 109: 4431.
6. Cohen B, Crespo-Hernandez CE, Kohler B (2004) Faraday Discuss 127: 137.
7. Cohen B, Hare PM, Kohler B (2003) J Am Chem Soc 125: 13594.
8. Crespo-Hernandez CE, Cohen B, Hare PM, Kohler B (2004) Chem Rev 104: 1977.
9. Crespo-Hernandez CE, Cohen B, Kohler B (2006) Nature 441: E8.
10. Crespo-Hernandez CE, Cohen B, Kohler B (2005) Nature 436: 1141.
11. Hare PM, Crespo-Hernandez CE, Kohler B (2007) Proc Natl Acad Sci USA 104: 435.
12. Malone RJ, Miller AM, Kohler B (2003) Photochem Photobiol 77: 158.
13. Pecourt JML, Peon J, Kohler B (2001) J Am Chem Soc 123: 10370.
14. Gustavsson T, Banyasz A, Lazzarotto E, Markovitsi D, Scalmani G, Frisch MJ, Barone V, Improta R (2006) J Am Chem Soc 128: 607.
15. Gustavsson T, Sarkar N, Lazzarotto E, Markovitsi D, Barone V, Improta R (2006) J Phys Chem B 110: 12843.
16. Gustavsson T, Sarkar N, Lazzarotto E, Markovitsi D, Improta R (2006) Chem Phys Lett 429: 551.
17. Gustavsson T, Sharonov A, Markovitsi D (2002) Chem Phys Lett 351: 195.
18. Markovitsi D, Talbot F, Gustavsson T, Onidas D, Lazzarotto E, Marguet S (2006) Nature 441: E7.
19. Onidas D, Markovitsi D, Marguet S, Sharonov A, Gustavsson T (2002) J Phys Chem B 106: 11367.
20. Santoro F, Barone V, Gustavsson T, Improta R (2006) J Am Chem Soc 128: 16312.
21. Sharonov A, Gustavsson T, Carre V, Renault E, Markovitsi D (2003) Chem Phys Lett 380: 173.
22. Sharonov A, Gustavsson T, Marguet S, Markovitsi D (2003) Photochem Photobiol Sci 2: 362.
23. He YG, Wu CY, Kong W (2004) J Phys Chem A 108: 943.
24. He YG, Wu CY, Kong W (2003) J Phys Chem A 107: 5145.
25. Fulscher MP, SerranoAndres L, Roos BO (1997) J Am Chem Soc 119: 6168.
26. Lorentzon J, Fulscher MP, Roos BO (1995) J Am Chem Soc 117: 9265.
27. Fulscher MP, Roos BO (1995) J Am Chem Soc 117: 2089.
28. Jean JM, Krueger BP (2006) J Phys Chem B 110: 2899.
29. Durbeej B, Eriksson LA (2002) J. Photochem Photobiol A-Chem 152: 95.
30. Zhang RB, Eriksson LA (2006) J Phys Chem B 110: 7556.
31. Canuel C, Elhanine M, Mons M, Piuzzi F, Tardivel B, Dimicoli I (2006) Phys Chem Chem Phys 8: 3978.

32. Blancafort L (2006) J Am Chem Soc 128: 210.
33. Chen H, Li SH (2006) J Chem Phys 124: 154315.
34. Serrano-Andres L, Merchan M, Borin AC (2006) Chem – Eur J 12: 6559.
35. Zendlova L, Hobza P, Kabelac M (2006) ChemPhysChem 7: 439.
36. Pancur T, Schwalb NK, Renth F, Temps F (2005) Chem Phys 313: 199.
37. Merchan M, Gonzalez-Luque R, Climent T, Serrano-Andres L, Rodriuguez E, Reguero M, Pelaez D (2006) J Phys Chem B 110: 26471.
38. Gustavsson T, Banyasz A, Lazzarotto E, Markovitsi D, Scalmani G, Frisch MJ, Barone V, Improta R (2006) J Am Chem Soc 128: 607.
39. Langer H, Doltsinis NL (2003) Phys Chem Chem Phys 5: 4516.
40. Langer H, Doltsinis NL (2004) Phys Chem Chem Phys 6: 2742.
41. Marian CM. (2007) J Phys Chem A 111: 1545.
42. Sobolewski AL, Domcke W (2004) Phys Chem Chem Phys 6: 2763.
43. Sobolewski AL, Domcke W, Hattig C (2005) Proc Natl Acad Sci USA 102: 17903.
44. Ismail N, Blancafort L, Olivucci M, Kohler B, Robb MA (2002) J Am Chem Soc 124: 6818.
45. Merchan M, Serrano-Andres L (2003) J Am Chem Soc 125: 8108.
46. Matsika S. (2004) J Phys Chem A 108: 7584.
47. Perun S, Sobolewski AL, Domcke W (2006) J Phys Chem A 110: 13238.
48. Zgierski MZ, Patchkovskii S, Fujiwara T, Lim EC (2005) J Phys Chem A 109: 9384.
49. Chen H, Li SH (2006) J Phys Chem A 110: 12360.
50. Perun S, Sobolewski AL, Domcke W (2005) Chem Phys 313: 107.
51. Schultz T, Samoylova E, Radloff W, Hertel IV, Sobolewski AL, Domcke W (2004) Science 306: 1765.
52. Abo-Riziq A, Grace L, Nir E, Kabelac M, Hobza P, de Vries MS (2005) Proc Natl Acad Sci USA 102: 20.
53. Perun S, Sobolewski AL, Domcke W (2006) J Phys Chem A 110: 9031.
54. Markwick PRL, Doltsinis NL, Schlitter J (2007) J Chem Phys 126: 045104.
55. Markwick PRL, Doltsinis NL (2007) J Chem Phys 126: 175102.
56. Canuel C, Mons M, Piuzzi F, Tardivel B, Dimicoli I, Elhanine M (2005) J Chem Phys 122: 074316.
57. Kang H, Lee KT, Jung B, Ko YJ, Kim SK (2002) J Am Chem Soc 124: 12958.
58. Mulkidjanian AY, Cherepanov DA, Galperin MY (2003) BMC Evol Biol 3: 12.
59. Ruzsicska BP, Lemaire DGE (1995) CRC handbook of organic photochemistry and photobiology, CRC Press, New York, p 1289.
60. Cadet J, Anselmino C, Douki T, Voituriez L (1992) J Photochem Photobiol B-Biol 15: 277.
61. Cadet J, Sage E, Douki T (2005) Mutat Res Funda Molec Mech Mutag 571: 3.
62. Dodonova NY. (1993) J Photochem Photobiol B-Biol 18: 111.
63. Gorner H. (1994) J Photochem Photobiol B-Biol 26: 117.
64. Szacilowski K, Macyk W, Drzewiecka-Matuszek A, Brindell M, Stochel G (2005) Chem Rev 105: 2647.
65. Eller MS, Ostrom K, Gilchrest BA (1996) Proc Natl Acad Sci USA 93: 1087.
66. Gorner H. (1991) J Photochem Photobiol B-Biol 10: 91.
67. Mitchell D (1995) In: Horspool W, Song P (ed) CRC handbook of organic photochemistry and photobiology, CRC Press, New York, p 1326.
68. Baik MH, Silverman JS, Yang IV, Ropp PA, Szalai VA, Yang WT, Thorp HH (2001) J Phys Chem B 105: 6437.
69. Kanvah S, Schuster GB (2006) Pure Appl Chem 78: 2297.

70. Yavin E, Boal AK, Stemp EDA, Boon EM, Livingston AL, O'Shea VL, David SS, Barton JK (2005) Proc Natl Acad Sci USA 102: 3546.
71. Crespo-Hernandez CE, Cohen B, Hare PM, Kohler B (2004) Chem Rev 104: 1977.
72. Sobolewski AL, Domcke W (2002) Eur Phys J D 20: 369.
73. Mishra SK, Shukla MK, Mishra PC (2000) Spectroc Acta Pt A-Molec Biomolec Spectr 56: 1355.
74. Mennucci B, Toniolo A, Tomasi J (2001) J Phys Chem A 105: 4749.
75. Broo A (1998) J Phys Chem A 102: 526.
76. Holmen A, Broo A, Albinsson B, Norden B (1997) J Am Chem Soc 119: 12240.
77. Wilson E, Decius J, Cross P (1955) Molecular vibrations, McGraw-Hill, New York.
78. Myers AB (1997) Acc Chem Res 30: 519.
79. Myers AB (1997) J Raman Spectrosc 28: 389.
80. Lee SY, Heller EJ (1979) J Chem Phys 71: 4777.
81. Kelley AM (1999) J Phys Chem A 103: 6891.
82. Myers AB, Mathies RA (1987) In: Spiro TG (ed) Biological Applications of Raman Spectroscopy, Wiley-Interscience, New York, p 1.
83. Myers AB (1995) In: Myers AB, Rizzo TR (ed) Laser Techniques in Chemistry, Wiley, New York, p 325.
84. Mukamel S (1995) Principles of nonlinear optical spectroscopy, Oxford University Press, New York.
85. Islampour R, Dehestani M, Lin SH (2000) Mol Phys 98: 101.
86. Hizhnyakov V, Tehver I (1997) J Raman Spectrosc 28: 403.
87. Gu Y, Champion PM (1990) Chem Phys Lett 171: 254.
88. Mahapatra S, Chakrabarti N, Sathyamurthy N (1999) Int Rev Phys Chem 18: 235.
89. Page JB, Tonks DL (1981) J Chem Phys 75: 5694.
90. Fraga E, Loppnow GR (1998) J Phys Chem B 102: 7659.
91. Webb MA, Kwong CM, Loppnow GR (1997) J Phys Chem B 101: 5062.
92. Loppnow GR, Fraga E (1997) J Am Chem Soc 119: 896.
93. Mathies R, Oseroff AR, Stryer L (1976) Proc Natl Acad Sci USA 73: 1.
94. Tsuboi M, Nishimura Y, Hirakawa A, Peticolas W (1987) In: Spiro TG (ed) Biological Applications of Raman Spectroscopy, vol 2. Wiley-Interscience, New York, p 109.
95. Benevides JM, Overman SA, Thomas GJ (2005) J Raman Spectrosc 36: 279.
96. Lagant P, Elass A, Dauchez M, Vergoten G, Peticolas WL (1992) Spectroc Acta Pt A-Molec Biomolec Spectr 48: 1323.
97. Mathlouthi M, Seuvre AM, Koenig JL (1984) Carbohydr Res 134: 23.
98. Wojcik MJ (1990) J Mol Struct 219: 305.
99. Florian J, Hrouda V (1993) Spectroc Acta Pt A-Molec Biomolec Spectr 49: 921.
100. Person W, Szczepaniak K (1993) Vib Spect Struct 20: 239.
101. Shanker R, Yadav RA, Singh IS (1994) Spectroc Acta Pt A-Molec Biomolec Spectr 50: 1251.
102. Tsuboi M, Ueda T, Ushizawa K, Sasatake Y, Ono A, Kainosho M, Ishido Y (1994) Bull Chem Soc Jpn 67: 1483.
103. Aamouche A, Ghomi M, Coulombeau C, Grajcar L, Baron MH, Jobic H, Berthier G (1997) J Phys Chem A 101: 1808.
104. Zhang SL, Michaelian KH, Loppnow GR (1998) J Phys Chem A 102: 461.
105. Rastogi VK, Singh C, Jain V, Palafox MA (2000) J Raman Spectrosc 31: 1005.
106. Nowak MJ (1989) J Mol Struct 193: 35.
107. Graindourze M, Smets J, Zeegershuyskens T, Maes G (1990) J Mol Struct 222: 345.
108. Person W, Szczepaniak K, Szczepaniak MDB,JE (1993) NATO ASI Ser C 406: 141.

109. Les A, Adamowicz L, Nowak MJ, Lapinski L (1992) Spectroc Acta Pt A-Molec Biomolec Spectr 48: 1385.
110. Szczepaniak K, Szczesniak MM, Person WB (2000) J Phys Chem A 104: 3852.
111. Colarusso P, Zhang KQ, Guo BJ, Bernath PF (1997) Chem Phys Lett 269: 39.
112. Susi H, Ard JS (1974) Spectroc Acta Pt A-Molec Biomolec Spectr A 30: 1843.
113. Lagant P, Vergoten G, Efremov R, Peticolas WL (1994) Spectroc Acta Pt A-Molec Biomolec Spectr 50: 961.
114. Rush T, Peticolas WL (1995) J Phys Chem 99: 14647.
115. Aida M, Kaneko M, Dupuis M, Ueda T, Ushizawa K, Ito G, Kumakura A, Tsuboi M (1997) Spectroc Acta Pt A-Molec Biomolec Spectr 53: 393.
116. Yarasi S, Billinghurst BE, Loppnow GR (2007) J Raman Spectrosc 38: 1117.
117. Peticolas WL, Rush T (1995) J Comput Chem 16: 1261.
118. Lagant P, Vergoten G, Peticolas WL (1999) J Raman Spectrosc 30: 1001.
119. Yarasi S, Brost P, Loppnow GR (2007) J Phys Chem A 111:5130.
120. Yarasi S, Brost P, Loppnow GR (2007 In preparation) To be submitted J Am Chem Soc.
121. Barnes AJ, Stuckey MA, Legall L (1984) Spectroc Acta Pt A-Molec Biomolec Spectr 40: 419.
122. Szczesniak M, Nowak MJ, Rostkowska H, Szczepaniak K, Person WB, Shugar D (1983) J Am Chem Soc 105: 5969.
123. Wojcik MJ, Rostkowska H, Szczepaniak K, Person WB (1989) Spectroc Acta Pt A-Molec Biomolec Spectr 45: 499.
124. Susi H, Ard JS (1971) Spectrochimica Acta Part A-Molecular Spectroscopy A 27: 1549.
125. Lewis TP, Miles HT, Becker ED (1984) J Phys Chem 88: 3253.
126. Chinsky L, Huberthabart M, Laigle A, Turpin PY (1983) J Raman Spectrosc 14: 322.
127. Nishimura Y, Tsuboi M, Kato S, Morokuma K (1981) J Am Chem Soc 103: 1354.
128. Chin S, Scott I, Szczepaniak K, Person WB (1984) J Am Chem Soc 106: 3415.
129. Letellier R, Ghomi M, Taillandier E (1987) Eur Biophys J Biophys Lett 14: 423.
130. Csaszar P, Harsanyi L, Boggs JE (1988) Int J Quantum Chem 33: 1.
131. Broo A, Pearl G, Zerner MC (1997) J Phys Chem A 101: 2478.
132. Ilich P, Hemann CF, Hille R (1997) J Phys Chem B 101: 10923.
133. Gaigeot MP, Sprik M (2003) J Phys Chem B 107: 10344.
134. Ghomi M, Letellier R, Taillandier E, Chinsky L, Laigle A, Turpin PY (1986) J Raman Spectrosc 17: 249.
135. Matsika S (2005) J Phys Chem A 109: 7538.
136. Matsika S (2004) J Phys Chem A 108: 7584.
137. Billinghurst BE, Loppnow GR (2006) J Phys Chem A 110: 2353.
138. Peticolas WL, Strommen DP, Lakshminarayanan V (1980) J Chem Phys 73: 4185.
139. Suen W, Spiro TG, Sowers LC, Fresco JR (1999) Proc Natl Acad Sci USA 96: 4500.
140. Toyama A, Takeuchi H, Harada I (1991) J Mol Struct 242: 87.
141. Fraga E, Billinghurst BE, Oladepo S, Loppnow GR (2007) In Preparation.
142. Billinghurst BE, Yeung R, Loppnow GR (2006) J Phys Chem A 110: 6185.
143. Budavari S (ed) (1989) The Merck Index : An Encyclopedia of Chemicals, Drugs, and Biologicals, Merck. Rathway, NJ: 11th ed.
144. Nishimura Y, Tsuboi M, Kubasek WL, Bajdor K, Peticolas WL (1987) J Raman Spectrosc 18: 221.
145. Tsuboi M, Komatsu M, Hoshi J, Kawashima E, Sekine T, Ishido Y, Russell MP, Benevides JM, Thomas GJ (1997) J Am Chem Soc 119: 2025.
146. Purrello R, Molina M, Wang Y, Smulevich G, Fossella J, Fresco JR, Spiro TG (1993) J Am Chem Soc 115: 760.

147. Pezolet M, Yu TJ, Peticolas WL (1975) J Raman Spectrosc 3: 55.
148. Blazej DC, Peticolas WL (1977) Proc Natl Acad Sci USA 74: 2639.
149. Nishimura Y, Hirakawa AY, Tsuboi M (1977) Chem Lett 907.
150. Nishimura Y, Tsuboi M, Kubasek WL, Bajdor K, Peticolas WL (1987) J Raman Spectrosc 18: 221.
151. Peticolas WL, Blazej DC (1979) Chem Phys Lett 63: 604.
152. Kubasek WL, Hudson B, Peticolas WL (1985) Proc Natl Acad Sci USA 82: 2369.
153. Blazej DC, Peticolas WL (1980) J Chem Phys 72: 3134.
154. Turpin PY, Peticolas WL (1985) J Phys Chem 89: 5156.
155. Peticola.Wl (1973) J Opt Soc Am 63: 477.
156. Blazej DC, Peticolas WL (1977) Proc Natl Acad Sci USA 74: 2639.
157. Fodor SPA, Rava RP, Hays TR, Spiro TG (1985) J Am Chem Soc 107: 1520.
158. Perno JR, Grygon CA, Spiro TG (1989) J Phys Chem 93: 5672.
159. Spiro TG (1974) Acc Chem Res 7: 339.
160. Behringer J (1975) Mol Spectrosc 3: 163.
161. Johnson BB, Peticolas WL (1976) Annu Rev Phys Chem 27: 465.
162. Tang J, Albrecht A (1970) Raman Spectrosc 2: 33.
163. Peticola Wl, Nafie L, Stein P, Fanconi B (1970) J Chem Phys 52: 1576.
164. Friedman JM, Hochstrasser RM (1973) Chem Phys 1: 457.
165. Warshel A, Karplus M (1972) J Am Chem Soc 94: 5612.
166. Inagaki F, Tasumi M, Miyazawa T (1974) J Mol Spectrosc 50: 286.
167. Garozzo M, Galluzzi F (1976) J Chem Phys 64: 1720.
168. Stein P, Miskowski V, Woodruff WH, Griffin JP, Werner KG, Gaber BP, Spiro TG (1976) J Chem Phys 64: 2159.
169. Nafie LA, Pastor RW, Dabrowiak JC, Woodruff WH (1976) J Am Chem Soc 98: 8007.
170. Mingardi M, Siebrand W (1975) J Chem Phys 62: 1074.
171. Shelnutt JA, Oshea DC, Yu NT, Cheung LD, Felton RH (1976) J Chem Phys 64: 1156.
172. Johnson BB, Nafie LA, Peticolas WL (1977) Chem Phys 19: 303.
173. Yarasi S, Yeung R, Loppnow GR (2007 In preparation for submission to) J Phys Chem A.
174. Kundu L, Loppnow GR (2007) Photochem Photobiol 83: 600.
175. Peticolas WL (1995) Methods Enzymol 246: 389.
176. Erfurth SC, Peticolas WL (1975) Biopolymers 14: 247.
177. Fodor SPA, Spiro TG (1986) J Am Chem Soc 108: 3198.
178. Mukerji I, Shiber MC, Fresco JR, Spiro TG (1996) Nucleic Acids Res 24: 5013.
179. Mukerji I, Shiber MC, Spiro TG, Fresco JR (1995) Biochemistry (NY) 34: 14300.
180. Chan SS, Austin RH, Mukerji I, Spiro TG (1997) Biophys J 72: 1512.
181. Grygon CA, Spiro TG (1990) Biopolymers 29: 707.
182. Schreier WJ, Schrader TE, Koller FO, Gilch P, Crespo-Hernandez CE, Swaminathan VN, Carell T, Zinth W, Kohler B (2007) Science 315: 625.